DOI:
10.1007/978-3-319-31744-1_17

Document Version
Peer reviewed version

An Automated Tensorial Classification Procedure for Left Ventricular Hypertrophic Cardiomyopathy

Santiago Sanz-Estébanez[1], Javier Royuela-del-Val[1], Susana Merino-Caviedes[1], Ana Revilla-Orodea[2], Teresa Sevilla[2], Lucilio Cordero-Grande[3], Marcos Martín-Fernández[1], and Carlos Alberola-López[1]

[1] Laboratorio de Procesado de Imagen, Universidad de Valladolid, Valladolid, España
{ssanest,jroyval,smercav}@lpi.tel.uva.es,{marcma,caralb}@tel.uva.es,
[2] I. de Ciencias del Corazón, Hospital Clínico Universitario, Valladolid, España
[3] Department Biomedical Engineering, King's College, London, U.K.
lucilio.cordero_grande@kcl.ac.uk

Abstract. *Cardiovascular diseases are the leading cause of death globally. Therefore, classification tools play a major role in prevention and treatment of these diseases. Statistical learning theory applied to magnetic resonance imaging has led to the diagnosis of a variety of cardiomyopathies states. We propose a two-stage classification scheme capable of distinguishing between heterogeneous groups of hypertrophic cardiomyopathies and healthy patients. A multimodal processing pipeline is employed to estimate robust tensorial descriptors of myocardial mechanical properties for both short-axis and long-axis magnetic resonance tagged images using the least absolute deviation method. A homomorphic filtering procedure is used to align the cine segmentations to the tagged sequence and provides 3D tensor information in meaningful areas. Results have shown that the proposed pipeline provides tensorial measurements on which classifiers for the study of hypertrophic cardiomyopathies can be built with acceptable performance even for reduced samples sets.*

Keywords: Magnetic Resonance Tagging · Fuzzy clustering · Support Vector Machines · Homomorphic Filtering · Harmonic Phase · Hypertrophic Cardiomyopathy · Least Absolute Deviation

1 Introduction

Classifications of heart muscle diseases have proved to be exceedingly complex and in many respects contradictory. Cardiomyopathies are an important and complex group of heart muscle diseases with multiple etiologies and heterogeneous phenotypic expression. Therefore, systematic classifications have traditionally been viewed as useful exercises that promote greater understanding of these diseases [1].

Hypertrophic cardiomyopathy (HCM) is very common and can affect people of any age. About one out of every 500 people has HCM. Men and women are

equally affected[2]. HCM is a common cause of sudden cardiac arrest in young people, including young athletes. Etiological factors are of great importance in cardiovascular disease detection [3]; specifically, genetic studies have been conducted in order to classify cardiomyopathies and to assess patients predisposition to suffer HCM [4, 5].

Imaging techniques provide essential descriptors for the study and classification of cardiomyopathies and, from them, cardiac magnetic resonance (MR) is increasingly becoming the standard technique as it provides information to assess the myocardial morphology, function and structure. Its use is especially relevant for quantitative analysis of myocardial motion, the anomalies of which are directly related with impaired cardiac function. From the set of MR acquisition techniques, MR-Tagging has become the reference modality for evaluating strain evolution in the human heart. This modality is based on the generation of a set of saturated magnetization planes on the imaged volume which may be subsequently tracked throughout the cardiac cycle [6], from which the cardiac function can be assessed. Harmonic Phase (HARP) based methods [7] are capable of reconstructing deformation fields accurately grounded on the assumption of constant local phase, which turns out to be more reliable than a constant pixel brightness assumption.

Global image-derived measures have been reported, such as the global longitudinal strain [8], which turns out to be an interesting tool that correlates with the global presence of fibrosis. A relation between extent of cardiac muscle cell disorganization and left ventricular wall thickness has also been established [9]; however, imaging studies focused on the characterization and classification of the nature of HCM are relatively scarce.

In order to provide greater understanding about these factors, comparative regional studies have been carried out in [10] for athletes, controls and HCM patients; the authors reveal a significant reduction in the diagonal components of the strain in HCM patients and athletes, but this reduction was not associated to any particular segment and it was even present in non-fibrotic regions. In [11] a local analysis is performed fusing the information of MR-Cine and Late Enhancement MR to provide more insight into the mechanical properties of the fibrotic tissue in HCM. Automated classifiers have been developed in [12] and [13] using global biomarkers derived from MR-Cine and electrocardiogram, respectively. Although the authors report noticeable prognostic values for the identification of different cardiovascular diseases, only global measures were used; however, local measurements may be of additional utility for the characterization of the fibrosis that accompanies primary/secondary HCM

In this paper we propose an automated processing pipeline to classify heterogeneous groups of HCM from myocardial functional descriptors obtained out of the deformation gradient tensor estimated from MR-Tagging images by means of a robust reconstruction method. We have applied different machine learning methods (supervised and unsupervised) using a sequential methodology that adapts to the characteristics of the subjects at every stage.

2 Materials and Methods

2.1 Materials

For the validation of the proposed approach on real data, we have performed cardiac studies in a population of 47 subjects, 23 of which are affected by primary HCM, 10 are affected by secondary HCM and the control group consists of 14 healthy volunteers.

A short axis (SA) MR-Tagging dataset, providing a coverage from apex to base, is acquired for each patient using a MR Complementary SPAtial Modulation of Magnetization (CSPAMM) SENSitivity Encoding (SENSE) Turbo Field Echo sequence on a Philips Achieva 3T scanner. Additionally, we have also acquired a SENSE balanced Turbo Field Echo SA MR-Cine sequence at the same spatial location for each patient, where the myocardium has been manually segmented at the end diastole (ED) phase. Segmentations are also used to define a region of interest on which to compute meaningful measures of the strain. Long axis (LA) MR-Tagging datasets and the corresponding MR-Cine sequence have also been acquired following the aforementioned acquisition protocol in each case. Additional details on these sequences are included in Table 1.

Table 1. Details on the sequences of MR images used in the paper. Δ_p : Spatial Resolution (mm). Δ_l : Slice Thickness (mm). N_p: Number of pixels along each direction. N_t: Number of Temporal Phases. N_s: Number of slices. T_R : Repetition Time (ms). T_E: Echo Time (ms). α: Flip Angle (°).

	Δ_p	Δ_l	N_p	N_t	N_s	T_R	T_E	α
MR-Tagging SA	1.21-1.32	10	256-432	16-25	10-15	2.798-6.154	1.046-3.575	7-25
MR-Cine SA	0.96-1.18	8-10	240-320	30	10-15	2.902-3.918	1.454-2.222	45
MR-Tagging LA	1.21-1.34	10	240-340	15-27	1-3	2.903-4.507	1.097-2.897	10-45
MR-Cine LA	0.98-1.25	8-10	256-448	30	1-3	2.858-3.529	1.251-2.132	45

2.2 Methods

The processing pipeline is divided in the following steps:

Alignment An alignment stage is performed with the purpose of mapping the MR-Cine segmentations provided by the cardiologist onto the MR-Tagging sequence. First, the temporal correspondence of the MR-Tagging images with the MR-Cine sequence is established by means of the DICOM timestamps; then, an affine registration method is performed to align MR-Tagging and MR-Cine images at the correct time instant. To that end, the MR-Tagging sequence is detagged following an homomorphic filtering procedure [14] to improve registration performance. Similar detagging procedures have been reported in [15] for global measures estimation. The proposed dettaging method is described below.

Let us assume a simple case in which an image $I(\mathbf{x})$ consists of an anatomical image $I_0(\mathbf{x})$(low-pass) multiplied by a tag pattern $f(\mathbf{x};\mathbf{g})$, where the gradient directions are given by $\mathbf{g} = [g_1, g_2]$. Our purpose is to estimate $I_0(\mathbf{x})$ from the final image $I(\mathbf{x})$. Our method is based on the assumption that the anatomical image shows a low variability, i.e., it can be considered a low pass signal. This principle is not always fulfilled as boundaries present sharp intensity changes. Consequently, we calculate the local mean of the image in order to alleviate the power smearing caused by the abrupt myocardium background transition and next, we separate anatomical and tag signals by applying the logarithm:

$$\log(I_n(\mathbf{x})) = \log(\overline{I}(\mathbf{x})) \approx \log I_0(\mathbf{x}) + \log f(\mathbf{x};\mathbf{g}) \; . \tag{1}$$

where $\overline{I}(\mathbf{x})$ denotes the local mean. The tag pattern term $\log f(\mathbf{x};\mathbf{g})$ has its energy localized at specific frequencies, while the term $\log I_0(\mathbf{x})$ is a low frequency signal. We can suppress the residual influence of the tag pattern using a notch filter on $\log(I_n(\mathbf{x}))$. The position of the spectral peaks can be easily estimated from the information obtained from the DICOM headers, so we have resorted to an isotropic Gaussian filter with radius r for every spectral peak detected. The filter bandwidth is normalized with respect to the wave number k of the applied modulation by using the parameter $\mu = r/k = 0.3$ according to [16].

The whole filtering pipeline is depicted in Figure 1:

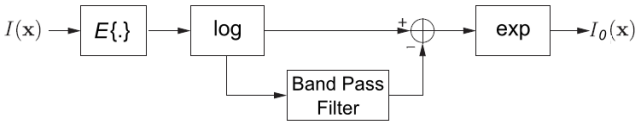

Fig. 1. Pipeline of homomorphic filtering procedure.

Estimation of the Material Deformation Gradient Tensor The estimation technique is based on the extraction of the local phase of the grid pattern according to the method presented in [16]. A windowed Fourier Transform (WFT) is applied to the image at the end-systole (ES) phase. The WFT provides a representation of the image spectrum in the surroundings of each pixel of the original image, so HARP Band Pass filtering techniques can be directly applied on the spatially localized spectrum of the image. The complex image can be reconstructed in the spatial domain by using an inverse discrete WFT (IWFT) prior to extract the phase.

As stated in [7], 3D HARP motion reconstruction using the SPAMM technique requires a minimum of 3 linearly independent wave vectors. In this paper we extend the aforementioned HARP methodology by allowing the application of a set of 4 wave vector (performing this estimation technique on CSPAMM

MR-Tagging LA and SA images), so 3D deformations can be robustly recovered, at least at the intersection points of both axes, applying the methodology presented in [17].

We can arrange the set of the four given wave vectors $\mathbf{k}_i^T$ in matrix form by:

$$\mathbf{K} = \left[\mathbf{k}_{1,SA}^T, \mathbf{k}_{2,SA}^T, \mathbf{k}_{1,LA}^T, \mathbf{k}_{2,LA}^T\right]^T \tag{2}$$

The material deformation gradient tensor $\mathbf{F}(\mathbf{x})$ is related to the gradient of the phase image $\phi_i(\mathbf{x})$ as stated in [7]. Rearranging the gradient of the phase images in matrix form as:

$$\mathbf{Y}(\mathbf{x}) = \left[\frac{\partial^* \phi_{1,SA}}{\partial \mathbf{x}^T}(\mathbf{x}), \frac{\partial^* \phi_{2,SA}}{\partial \mathbf{x}^T}(\mathbf{x}), \frac{\partial^* \phi_{1,LA}}{\partial \mathbf{x}^T}(\mathbf{x}), \frac{\partial^* \phi_{2,LA}}{\partial \mathbf{x}^T}(\mathbf{x})\right]^T, \tag{3}$$

we obtain the material deformation gradient $\mathbf{F}(\mathbf{x})$ from:

$$\mathbf{K} = \mathbf{Y}(\mathbf{x})\mathbf{F}(\mathbf{x}). \tag{4}$$

In order to estimate $\mathbf{F}(\mathbf{x})$, one could resort to the Least Squares (LS) method. However, bearing in mind that HARP-like methods suffer phase interferences (especially within the vicinity of boundaries), which give rise to outliers , our proposal is to resort to the Least Absolute Deviation (LAD) method, due to its robustness [17]. Hence, the reconstruction is performed iteratively by:

$$\mathbf{F}_{l+1}(\mathbf{x}) = (\mathbf{Y}^T(\mathbf{x})\mathbf{W}_l(\mathbf{x})\mathbf{Y}(\mathbf{x}))^{-1}\mathbf{Y}^T(\mathbf{x})\mathbf{W}_l(\mathbf{x})\mathbf{K}, \tag{5}$$

with $\mathbf{W}_l(\mathbf{x})$ a diagonal weight matrix obtained by:

$$W_l^{jj}(\mathbf{x}) = \frac{1}{\sqrt{\sum_{h=1}^{3}\left(K^{jh} - \sum_{g=1}^{3} Y^{jg}(\mathbf{x})F_l^{gh}(\mathbf{x})\right)^2}} \tag{6}$$

and initially establishing $\mathbf{F}_0(\mathbf{x}) = \mathbf{I}$, with $\mathbf{I}$ the identity matrix.

Once $\mathbf{F}(\mathbf{x})$ is reconstructed, the Green-Lagrange strain tensor can be easily obtained as: $\mathbf{E}(\mathbf{x}) = 1/2(\mathbf{F}^T(\mathbf{x})\mathbf{F}(\mathbf{x}) - \mathbf{I})$.

Classification Mechanical descriptors are extracted from the aforementioned tensors. We considered the projected components of the strain tensor on the usual radial-circumferential-longitudinal $\{r, c, l\}$ space. These components will be referred to as E^{ab}, where a and b will be components of this space. In all the cases, all the features will be averaged within three areas in the heart along its LA; specifically, we will consider components at the base, mid-ventricle and apex. On the other hand, we will also calculate the curl of the deformation field as a measure of rotation. We will generically refer to the twist as the unsigned difference between two components that measure rotation [18], one at the base, the second one at the apex. When we refer to the rotation modulus, the specific

component will be the unsigned average of the component in the mid-ventricle area. Additionally, since some rotation-related components have opposite directions in apex and base, we will consider the location of the zero crossing for these components.

Once the principal heart motion descriptors have been calculated, a normalization stage [19] is applied in order to diminish the influence of possible outliers. A sigmoidal function is used to this end; data are mapped on the interval $(0, 1)$.

Our purpose is to classify a sample into one of three classes, namely, control, primary HCM and secondary HCM. Since secondary HCM patients have subtle differences with respect to the other two classes, we have resorted to a two-stage classification procedure (see Fig. 2). At the first stage we grossly pursue to distinguish between controls and primary HCM. Secondary HCM patients will fall on either of the two mentioned partitions. As for the second stage the purpose is to tell apart controls and secondary HCM, on one hand, and primary and secondary HCM, on the other hand. Notice that primary HCM patients incorrectly classified as a control in the first stage (or vice versa) will not be correctly classified; however, as we will describe later, this situation hardly takes place.

Optimal feature selection and classification are intimately related; those features whose classification figures are the highest are considered as the optimal features for that classification stage. To minimize overtraining, despite the reduced sample size, a Leave-10-out cross validation procedure has been used and data samples have been randomized; the proportions of control/primary/secondary have been kept unaltered along trials. For every trial we record the feature set with best performance; after one hundred trials we can identify the feature vector that has been selected the most; this will be the chosen one for the classification stage. As for finding classification performance, the procedure is repeated with a new randomized Leave-10-out procedure using the aforementioned selected feature vector as the input. In all the cases, 3-component feature vectors have been tested. Higher dimensionality has been tried but with no improve in performance.

The procedure described above has been carried out using Fuzzy c-Means (FCM) [20] and Support Vector Machines [21] both with quadratic (SVMq) and Gaussian (SVMg) kernels [22]. We have also tested a combination of them at different stages. As for the fuzzy clustering, the method requires that a threshold is set for the membership grade of each partition to carry out a final hard threshold. This value is another parameter that has to be optimized.

As for the first stage, the selected features are the ones that provide the highest accuracy involving only healthy and primary HCM. The modulus of E^{cc} and curl as well as the twist of the curl of the 2D deformation field[18] have proven to provide a good separability between these groups for each one of the tested classification techniques.

Then, for both output partitions of the first stage, another classification is established with the purpose of detecting secondary HCM cases in groups of healthy volunteers and primary HCM, respectively. The objective of this stage

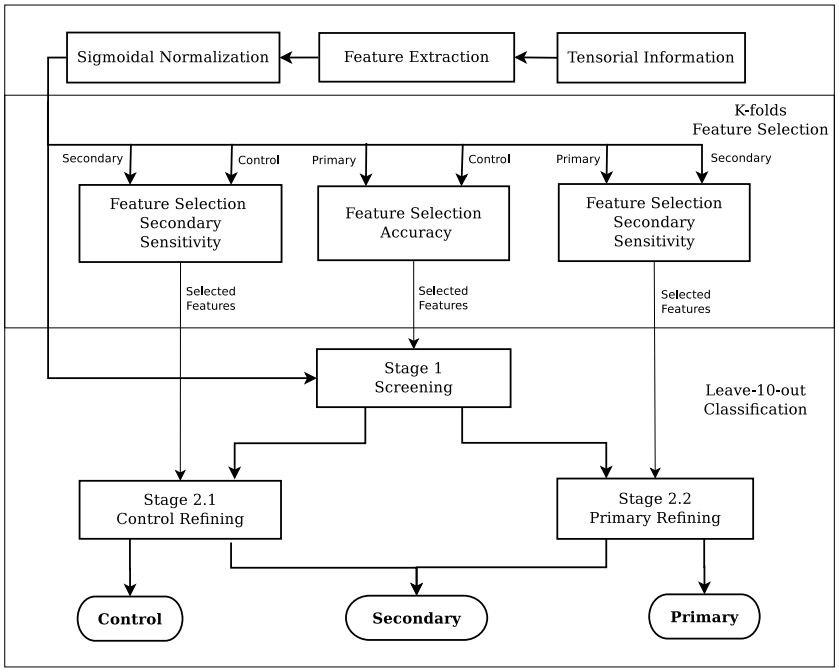

Fig. 2. Pipeline of the feature selection and classification stages.

is to increase the classifier sensitivity with respect to secondary HCM cases; if several feature vectors share the maximum sensitivity with respect to this group, we select the feature vector with maximum specificity (i.e., with maximum sensitivity with respect to the other class, controls in classifier 2.1 and primaries in classifier 2.2, following the notation in Figure 2).

It turns out that the selected feature vector for classifier 2.2 consists of E^{lc} and E^{rc} components in mid-ventricular slices and E^{ll} over basal slices for the FCM analysis; for both SVM analyses, zero crossing of E^{rc} component as well as the curl of the 2D deformation field substitute the components E^{ll} and E^{rc}. On the other hand, for the 2.1 classifier, higher variability was found. Modulus of E^{cc} and E^{rr} components in the mid-ventricular area as well as the twisting obtained from eigenvector shift [18] were used in the SVMg analysis, while for SVMq the latter was replaced by the twisting given by the principal directions tangent angle [18]. As for FCM analysis, E^{cc} modulus, curl zero crossing and its modulus have been accounted for.

3 Results

3.1 Alignment

For the homomorphic filtering procedure, the validation is performed in terms of contour overlapping, measured by means of the Dice Coefficient [23]. Different

affine registration procedures have been performed in order to align MR-Cine image at ED phase with its corresponding in the original MR-Tagging and the filtered sequences. The resulting transformation is applied to the MR-Tagging segmentation at ED phase and the Dice coefficient is calculated between the latter and the original MR-Cine segmentation. Boxplot diagrams of the Dice coefficient distributions obtained with the three similarity metrics compared are displayed in Figure 3.

Mann-Whitney U-tests have been used to determine whether significant improvements exist in the medians of the Dice coefficient distributions when carrying out the homomorphic filtering stage; three different metrics have used, the results of which are, p= 0.0154 for cross-correlation [24], p=2.03×10^{-11} for mutual information and p= 0.0134 for sum of squares; consequently, in the three cases significant differences have been observed.

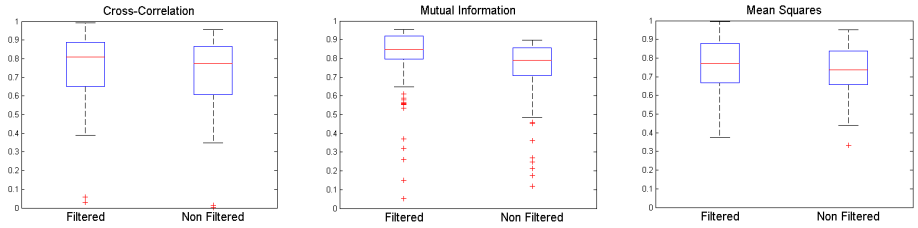

Fig. 3. Boxplot diagrams of the Dice Coefficient for different registration methods with and without homomorphic filtering.

3.2 Tensorial Estimation

For each patient described in Section 2.1, 3D deformation gradient tensors are obtained from the LS and the LAD methods; the 2D components of these tensors (i.e., excluding the five terms related to the longitudinal component) should ideally be equal to the components of the 2D tensor obtained directly from the MR-Tagging SA images. So, since in the 2D case four parameters are estimated out of two orientations and in 3D nine are estimated out of four, we take the 2D tensor as the reference and measure the quality of the estimator in 3D as the similarity between its 2D components with those of the 2D tensor. Similarity is calculated in terms of the Frobenius norm difference (FND) [17] between the 2D tensor and its correspondence in the 3D tensor.

Figure 4 shows the distribution of the FND indexed for each of the methods used for the 3D tensor estimation (left) as well as the corresponding FND Cumulative Distribution Function (CDF) (right). Significant differences have been found between medians of both error distributions by means of the Mann-Whitney U-test (p=8.94×10^{-22}).

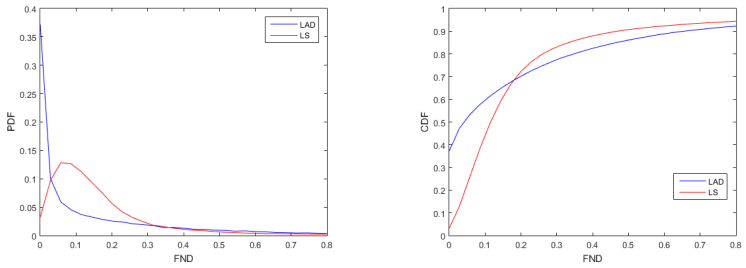

Fig. 4. FND and CDF of the tensors obtained by either LAD or LS reconstruction method with respect to the 2D tensor reconstructed with minimal wave vectors.

3.3 Classification

Finally, we show the performance of the classification algorithm in Table 2 by means of normalized confusion matrices. Each column of the matrix represents the instances in the predicted class, while each row represents the instances in the actual class. This allows more detailed analysis than mere proportion of correct guesses (accuracy).

From Table 2 global accuracy as well as measures of specificity and sensitivity can be obtained for each group and each classification method. The approach referred to as *mixed* consists of FCM in stages 1 and 2.2 and SVMg in stage 2.1.

Table 2. Confusion matrices for the FCM, SVMq, SVMg and *mixed* classifers.

	FCM			SVMq			SVMg			Mixed		
	Con	Sec	Pri	Con	Sec	Pri	Con	Sec	Pri	Con	Sec	Pri
Con	0.245	0.055	0	0.225	0.072	0.003	0.215	0.085	0	0.239	0.061	0
Sec	0.051	0.125	0.024	0.063	0.136	0.001	0.08	0.119	0.001	0.036	0.147	0.017
Pri	0.012	0.016	0.472	0	0.148	0.352	0.004	0.069	0.427	0	0.034	0.466

4 Discussion

In Section 3.1 we have described an alignment stage aimed at mapping the MR-Cine segmentations provided by cardiologist onto the MR-Tagging sequence. The segmentations are used to define a region of interest on which to compute meaningful measures of the tensor. This stage could be performed for every cardiac phase as MR-Cine sequence has been preprocessed by means of a groupwise elastic registration procedure in order to propagate the ED segmentations along the whole cardiac cycle.

Figure 3 shows an increase in the overlapping of the segmentations when the homomorphic filter is applied to the image independently of the metric used in

the registration procedure; specifically, the improvement in performance caused by the homomorphic filter is higher than the improvement obtained by switching the registration metric. Therefore, we can conclude that a preprocessing stage is relevant in order to perform precise registration over MR-Tagging images.

Although in this paper the ultimate goal of the alignment stage is the projection of segmentations, this stage can be also applied to other more ambitious objectives, such as a multimodal scheme of material point tracking along the cardiac cycle or finding the association between gadolinium accumulation in late enhancement images and local mechanical abnormalities in the myocardium. We have taken some steps in this latter direction [11, 25].

As for the tensor estimation technique, a better response in terms of robustness is observed in Figure 4 for the LAD estimator with respect to LS. The results conclusively support the hypothesis that the LAD estimator is better suited for this reconstruction problem, where the main source of inconsistencies seems to be the presence of phase interferences as opposed to the presence of noise in the measurements. Specifically, the CDF curve is left skewed although heavier tails are observed, i.e., the majority of the estimations are more accurate than for the LS method, at the expense of the onset of larger errors whenever estimations are inaccurate.

From the results in Section 3.3 we can see that the methodology here presented seems effective in classifying HCM patients out of tensorial descriptors obtained from MR-Tagging sequences. Better sensitivity figures are observed for both control and primary HCM patients with respect to the secondary patients, for which performance is clearly lower (specially for SVMq), possibly due to the small data sample included in the study for this group. A poor sensitivity to primary HCM is observed when using SVMq, resulting in the lowest global accuracy. A quadratic kernel seems inadequate for this problem, possibly due to the multiple states present in primary HCM. On the other hand, SVMg provides best performance in detecting secondary HCM. Consequently, we have resorted to a *mixed* approach to take advantage of the accuracy in primary HCM detection of FCM analysis and the secondary HCM sensitivity shown by SVMg, obtaining sensitivity figures higher than 70% for each group (especifically, 80% for control, 73%for secondary patients and 93% for primary patients). It is worth mentioning that no primaries as classified as controls and vice versa; therefore, the pipeline proposed seems a proper screening tool.

5 Conclusion

A processing pipeline for the tensorial classification of hypertrophic cardiomyopathies is presented which builds upon a robust 3D tensor estimation technique from SA and LA MR-Tagging sequences and a novel homomorphic filtering preprocessing step. This filtering method has significantly improved the accuracy of the alignment and it paves the way to construct multimodal processing schemes in which different modalities can be accurately dealt with, as it would be the case for MR-Cine, MR-Tagging and Late Enhancement MR.

A comparative study in terms of robustness provided by LAD and LS estimators in real datasets has also been carried out, supporting the hypothesis that LAD estimator is worth taking for an overdetermined reconstruction problem in tagging images.

For the classifier itself, we have compared three different classification methods used in machine learning, namely, FCM and SVM with quadratic and Gaussian kernels. We have shown that the fuzzy approach provides better global accuracy results although it is not suitable for small data sets, while SVM do. Consequently, we have resorted to a mixed approach that takes advantage of both techniques obtaining high rates in global accuracy with more balanced sensitivities of each class with respect to those obtained with a unique classifier in the sequential procedure.

Although our classifier is designed for HCM patients, it can be easily tuned for other cardiovascular diseases as long as appropiate biomarkers are available; these biomarkers could be derived from different technologies.

Acknowledgments. This work was partially supported by the Spanish Ministerio de Ciencia e Innovacion under Research Grant TEC2013-44194-P, the Spanish Ministerio de Ciencia e Innovacion and the European Regional Development Fund (ERDF-FEDER) under Research Grant TEC2014-57428-R and the Spanish Junta de Castilla y Leon under Grant VA136U13.

References

1. Baron, B.J.: The 2006 American Heart Association Classification of Cardiomyopathies Is the Gold Standard. Circ. Heart Fail. 1, 72–76 (2008)
2. Hypertrophic cardiomyopathy. `http://www.heart.org/HEARTORG/Conditions/More/Cardiomyopathy/Hypertrophic-Cardiomyopathy_UCM_444317_Article.jsp#.Vkyih3YvdD8`, accessed: 2015-11-18
3. Karamitsos, T.D., Neubauer, S.: The interplay between cardiac strain and fibrosis in non-ischaemic cardiomyopathies: insights from cardiovascular magnetic resonance. Eur J Heart Fail 13, 927–928 (2011)
4. Richard, P., Charron, P., Carrier, L., Ledeuil, C., Cheav, T., Pichereau, C., Benaiche, A., Isnard, R., Dubourg, O., Burban, M., Gueffet, J.P., Millaire, A., Desnos, M., Schwartz, K., Hainque, B., Komajda, M.: Hypertrophic Cardiomyopathy: Distribution of Disease Genes, Spectrum of Mutations, and Implications for a Molecular Diagnosis Strategy. Circulation 107, 2227–2232 (2003)
5. Braunwald, E., Seidman, C.E., Sigwart, U.: Contemporary Evaluation and Management of Hypertrophic Cardiomyopathy. Circulation 106, 1312–1316 (2002)
6. Shehata, M.L., Cheng, S., Osman, N.F., Bluemke, D.A., Lima, J.A.: Myocardial tissue tagging with cardiovascular magnetic resonance. J Cardiovasc Magn Reson 11, 55 (2009)
7. Osman, N.F., McVeigh, E.R., Prince, J.L.: Imaging heart motion using harmonic phase MRI. IEEE Trans Med Imaging March 19(3), 186–202 (2000)
8. Shimon, A., Reisner, M.D., Lysyansky, P., Agmon, Y., Mutlak, D., Lessick, J., Friedman, Z.: Global Longitudinal Strain: A Novel Index of Left Ventricular Systolic Function. J Am Soc Echocardiogr 17, 630–633 (2000)

9. Maron, B.J., Wolfson, J.K., Roberts, W.C.: Relation Between Extent of Cardiac Muscle Cell Disorganization and Left Ventricular Wall Thickness in Hypertrophic Cardiomyopathy. The American Journal of Cardiology 70, 785–790 (1992)
10. Piella, G., De Craene, M., Bijnens, B.H., Tobon-Gómez, C., Huguet, M., Avegliano, G., Frangi, A.F.: Characterizing myocardial deformation in patients with left ventricular hypertrophy of different etiologies using the strain distribution obtained by magnetic resonance imaging. Rev Esp Cardiol 63, 1281–1291 (2010)
11. Cordero-Grande, L., Sevilla, T., Revilla, A., Martín-Fernández, M., Alberola-López, C.: Assessment of the Fibrotic Myocardial Tissue Mechanics by Image Processing. Computing in Cardiology Conference pp. 635–638 (2013)
12. Gopalakrishnan, V., Menon, P.G., Madan, S.: cMRI-BED: A novel informatics framework for cardiac MRI biomarker extraction and discovery applied to pediatric cardiomyopathy classificationn. In: 2nd International Work-Conference on Bioinformatics and Biomedical Engineering. Granada, Spain (2014)
13. Rahman, Q.A., Tereshchenko, L.G., Kongkatong, M., Abraham, T., Abraham, M.R., Shatkay, H.: Utilizing ECG-Based Heartbeat Classification for Hypertrophic Cardiomyopathy Identification. IEEE Trans Nanobioscience 14, 505–512 (2015)
14. Aja-Fernández, S., Pieçiak, T., Vegas-Sánchez-Ferrero, G.: Spatially variant noise estimation in MRI: A homomorphic approach. Medical Image Analysis 20, 184–197 (2014)
15. Makram, A., Khalifa, A., El-Rewaidy, H., Fahmy, A., Ibrahim, E.S.H.: Assessment of Global Cardiac Function from Tagged Magnetic Resonance Images. Comparison with Cine MRI. In: 23rd Proceedings of the International Society on Magnetic Resonance in Medicine. vol. 23, p. 4472. Toronto, Canada (2015)
16. Cordero-Grande, L., Vegas-Sánchez-Ferrero, G., Casaseca-de-la-Higuera, P., Alberola-López, C.: Improving harmonic phase imaging by the windowed Fourier transform. In: 8th IEEE International Symposium on Biomedical Imaging: From Nano to Macro. pp. 520–523. Chicago, USA (2011)
17. Cordero-Grander, L., Royuela-del-Val, J., Sanz-Estébanez, S., Martín-Fernández, M., Alberola-López, C.: Multi-Oriented Windowed Harmonic Phase Reconstruction for Robust Cardiac Strain Imaging. Med. Image Anal. in press (2015)
18. Fung, Y.C.: Foundations of Solid Mechanics. Prentice-Hall, Englewood Cliffs, NJ (1965)
19. Theodoridis, S., Koutroumbas, K.: Pattern Recognition. Academic Press, San Diego (1999)
20. Bezdec, J.C.: Pattern Recognition with Fuzzy Objective Function Algorithms. Plenum Press, New York (1981)
21. Cortes, C., Vapnik, V.: Support-Vector Networks. Machine Learning 20, 273–297 (1995)
22. Vert, J.P., Tsuda, K., Schölkopf, B.: A primer on kernel methods. Kernel Methods in Computational Biology pp. 1–42 (2004)
23. Dice, L.R.: Measures of the Amount of Ecologic Association Between Species. Ecology 26, 297–302 (1945)
24. Avants, B.B., Epstein, C.L., Grossman, M., Geel, J.C.: Symmetric Diffeomorphic Image Registration with Cross-Correlation: Evaluating Automated Labeling of Elderly and Neurodegenerative Brain. Med. Image Anal. 12, 26–41 (2008)
25. Sanz-Estébanez, S., Merino-Caviedes, S., Sevilla, T., Revilla-Orodea, A., Martín-Fernández, M., Alberola-López, C.: Cardiac Strain Assessment for Fibrotic Myocardial Tissue Detection in Left Ventricular Hypertrophic Cardiomyopathy. In: Congreso Anual de la Sociedad Española de Ingeniería Biomédica. pp. 10–13. Madrid, Spain (2015)